

LONG, T., WANG, S., CAO, W., ZHOU, H., FERNANDEZ, C. and WANG, Y. 2023. A novel M-1 structured bidirectional long short term memory-rauch Tung Striebel smoothing algorithm for the joint estimation state of charge and multi-constrained sustained peak power of lithium-ion batteries. *Journal of energy storage* [online], 67, article number 107576. Available from: <https://doi.org/10.1016/j.est.2023.107576>

# A novel M-1 structured bidirectional long short term memory-rauch Tung Striebel smoothing algorithm for the joint estimation state of charge and multi-constrained sustained peak power of lithium-ion batteries.

LONG, T., WANG, S., CAO, W., ZHOU, H., FERNANDEZ, C. and WANG, Y.

2023

# A novel M-1 structured Bidirectional Long Short Term Memory-Rauch Tung Striebel Smoothing algorithm for the joint estimation State of Charge and multi-constrained sustained peak power of lithium-ion batteries

Tao Long<sup>a,b</sup>, Shunli Wang<sup>a,b,\*</sup>, Wen Cao<sup>a</sup>, Heng Zhou<sup>a,b</sup>, Carlos Fernandez<sup>c</sup>, Yangtao Wang<sup>a,b</sup>

<sup>a</sup> School of Information Engineering, Southwest University of Science and Technology, Mianyang 621010, China

<sup>b</sup> College of Electrical Engineering, Sichuan University, Chengdu 610065, China

<sup>c</sup> School of Pharmacy and Life Sciences, Robert Gordon University, Aberdeen AB10-7GJ, UK

\* Corresponding author at: School of Information Engineering, Southwest University of Science and Technology, Mianyang 621010, China.  
E-mail address: wangshunli1985@qq.com (S. Wang).

## A B S T R A C T

The estimation of State of Charge (SoC) and State of Power (SoP) of lithium-ion batteries is an important part of battery management system. For the purpose of obtaining high-precision SoC and SoP estimation results, this paper proposes a novel M-1 structured Bidirectional Long Short Term Memory-Rauch Tung Striebel Smoothing (BiLSTM-RTSS) algorithm, which can effectively fit current, voltage, temperature and SoC by using the improved sliding window M-1 technique. The RTSS algorithm is applied to update the SoC estimation of the BiLSTM to facilitate the accuracy and speed of SoC estimation. Subsequently, to better estimate the SoP with duration of 30 s, 2 min, and 4 min, three key constraints including SoC estimation results, second-order RC model and battery limits, are simultaneously used in SoP estimation. According to experiment, the mean absolute error of SoC is 0.602, 0.619 and 0.548, 0.469 respectively, under the conditions of HPPC and BBST. When the duration is 30s, the peak charging and discharging currents up to 170 A and 380 A. In addition, the estimation trends of sustained peak power and peak current are in the same direction. The experimental results verify the rapidity and reliability of the proposed algorithm for SoC and SoP.

### Keywords:

Bidirectional Long Short Term Memory; Rauch Tung Striebel Smoothing; Multiple constraints; Joint estimation; M-1 structured; Forward and backward

## 1. Introduction

At present, the national economy is rapidly growing, and the demand for fossil energy is increasing [1]. The concomitant result is that the threat of energy depletion is earlier and more severe [2,3]. With the twin economic energy shortage and environmental degradation problems, many countries have invested many financial and human resources in researching and promoting new energy sources to relieve energy pressure [4,5]. The withdrawal of traditional fuel vehicles has become an inevitable trend, and the development of electric vehicles will be unstoppable [6,7]. Among them, Lithium-ion batteries are the most widely used in the new energy electric vehicles field because of their high energy density, high output power, and high-cost performance [8]. Therefore it is essential to establish a reliable Battery Management System (BMS) to accurately and safely monitor the various performance indicators of lithium-ion batteries [9]. The estimation monitoring of the State of Charge (SoC) and State of Power (SoP) in the BMS and how to improve the accuracy of SoC estimation is a hot research topic in BMS [10]. For instance, the impact of SoC and SoP estimation results on the control and safety of electric vehicles [11].

Many researchers have published corresponding research papers for the hot research topics of SoC estimation. Initially, model-based approaches are prevalent. Xiong et al. designed an adaptive improved Ampere hour (Ah) formula and the complete SoC estimation model to update the value in real-time [12]. Zhou et al. indicated a fast Open Circuit Voltage (OCV) estimation method to estimate SoC results, which only needs accurate OCV data [13]. Liu et al. used the Extended Kalman filter (EKF) algorithm to estimate the SoC by collecting terminal voltage of each lithium-ion batteries [14]. Gholizadeh et al. developed a systematic approach to estimate SoC based on the adaptive observers to determine the covariance matrix of parameter noise in the EKF [15]. Huang et al. applied the Unscented Kalman filter (UKF) algorithm to solve the non-linearity problem efficiently and used it to describe the battery degradation capacity [16].

Second, machine learning and deep learning approaches can ignore the effects of models and fit large amounts of lithium-ion battery charge and discharge data to SoC [17], simplifying the process of model estimation and further attracting the attention of most academics [18,19]. Jafari et al. used voltage-time data as input and an extreme gradient boosting algorithm for SoC estimation of lithium-ion batteries [20]. Shen et al. proposed the concepts of transfer learning and ensemble learning, which target applications with only a relatively small training dataset to get highly accurate estimation results [21]. Hannan et al. presented the capacity of optimized machine learning techniques toward enhanced SoC estimation in terms of learning capability, accuracy, generalization performance, and convergence speed [22]. Liu et al. proposed a method to estimate the SoC of lithium-ion batteries with a Temporal Convolutional Network (TCN) [23]. Chen et al. used a recurrent neural network called gated recurrent unit network based on genetic algorithm (GA-GRU) [24]. Zhao et al. combined recursive neural networks (RNN) and convolutional neural networks (CNNs) that improve battery data representation and fully extract feature information to estimate SoC [25]. Bian et al. constructed a Stacked Bidirectional Long Short Term Memory (SBLSTM) neural network capable, which can capture battery time information in forward and backward directions [26].

Third, the current research on SoP is not deeper than SoC research. Generally, SoP estimates results under multiple constraints, the difference being in the different constraints [27]. In addition, SoC and SoP estimate results often based on a co-estimation method [28]. Tan et al. indicated constraints including current, voltage and SoC to quickly calculate SoP, which the SoC is estimated based on the EKF algorithm [29]. Liu et al. estimated SoP based on the fractional order equivalent circuit model, where the SoC was obtained by curve fitting [30]. Qin et al. proposed a new co-estimation method of SoC-SoP based on the electro-thermal model and UKF algorithm [31]. Shu et al. designed a temperature compensation-based adaptive algorithm to estimate SoC, State of Health (SoH) and SoP, which used adaptive extended Kalman filter and multi constraints subject to obtain SoC and SoP [32]. Zhang et al. proposed a systematic co-estimation framework to co-estimation SoC and SoP based on UKF algorithm and OCV model [33].

Finally, several new algorithms are being developed. Sun et al. proposed a model combining incremental capacity analysis and Bidirectional Long Short Term Memory neural networks based on health characteristic parameters [34]. Fan et al. proposed a novel Long Short Term Memory network combined with an adaptive unscented Kalman filter (LSTM-AUKF) method that can estimate SoC and State of Energy (SoE) at the same time [35]. Li et al. proposed an optimized forecasting model—an extreme learning machine (ELM) model coupled with the heuristic Kalman filter (HKF) algorithm to forecast the capacity of supercapacitors [36]. However, new research still needs to be done for SoP.

According to the above analysis, the estimation SoC can be divided into model-based, machine learning, deep learning and a combined model data-driven method. For SoP estimation methods, it can be divided into based on current, voltage, SoC and multi-parameter constraints methods.

Different algorithms have different advantages and disadvantages. The model-based algorithm is highly dependent on the choice of the battery model. However, lithium-ion batteries tend to have a complex operating environment and variable internal states, so model-based algorithms often need to be more generalizable and usually require multiple validations [12]. In comparison, machine learning and deep learning methods can ignore the effects of models and fit large data [37]. Nevertheless, this method takes a lot of time to fit data and adjust the hyperparameters, with overfitting and underfitting in the process [38]. In contrast, the combined model data-driven approach does not require long fitting times and frequent parameter adjustments, but a suitable model-based algorithm is needed to match, so incorrect algorithm selection will not improve the estimation accuracy [39]. Based solely on a single current, voltage and SoC conditions often result in large errors, leading to overcharging or over discharging batteries. By contrast, multi-parameter constraints can limit peak power and current through various factors, but often with poor constraint results due to need for accurate SoC estimation results and a stable and reliable model.

In the above algorithms, the LSTM and multi-constraints algorithm can effectively estimate SoC and SoP of lithium-ion batteries [40]. First, the unique forgetting gate structure of LSTM can estimate SoC by forgetting a portion of the data to avoid overfitting. Second, the SoC results are used as one of the multi-constraints to obtain the final SoP estimate. Thus similar SoC estimation methods are widely used [41].

Despite this information, using LSTM and multi-constraint methods to directly estimate SoC and SoP is still a difficult task. Firstly, using LSTM to predict SoC will take a lot of time. Secondly, most of times using a combined neural network and model approach will lead to insignificant results. Finally, traditional SoP estimation methods often do not consider the peak power output at long sustained times. Most importantly, reasonable SoC estimates for SoP estimation need to be obtained quickly. Unfortunately, this is difficult to achieve in practice.

To address the above research gaps, a novel fusion algorithm based on neural network and model is proposed, which includes M-1 structured Bidirectional Long Short Term Memory and Rauch Tung Striebel smoother algorithm. Besides this, a multi-constraint algorithm was designed to estimate the peak power at long sustained time. The main contributions of the paper are below.

- (1) This paper designs a many-to-one Bidirectional Long Short Term Memory (BiLSTM) algorithm, using a sliding window technique to strengthen the correlation between the data, which uses the previous moment's data to revise the next moment's estimation results, greatly improving the accuracy of the estimation.
- (2) A Rauch Tung Striebel Smoothing (RTSS) algorithm is used to optimize BiLSTM. Through this method. The algorithm can reduce the training time of the BiLSTM and does not consider the fluctuation of the results.
- (3) Using a multi-constraint algorithm to estimate peak current and peak power. Considering the practicalities of vehicle operation, this paper establishes a continuous peak current and peak power estimation method, including the 30s, 2 min, and 4 min.

## 2. Mathematical analysis

### 2.1. Improved bidirectional long short-term memory neural network

The LSTM was proposed to solve the gradient disappearance and gradient explosion problems, and it can effectively connect the past and present data. In the early period, its design was inspired by the various logic gates in computers. The individual cells of the LSTM, as shown in Fig. 1.

Similar to the various computer gates, three kinds of gates can be divided into the LSTM algorithm. Which are the output gate, input gate, and forget gate, respectively. The gate used to control the output and input data is called the output gate and input gate. Common neural networks algorithm will transfer useless history data to the next moment, leading to a large error in the output of the iteration result. However, LSTM can use forget gate for dealing with useless history data to solve the problem. This design can effectively enable some data to be preserved and others to be forgotten.

In Fig. 1, the input gate, forget gate, and output gate are calculated as follows. In the LSTM gate, the data includes input at the current time and the hidden state at the previous time. They are handled by three sigmoid fully connected layers, represented in the figure as  $\sigma$ , and the values are between 0 and 1. Suppose the number of hidden cells is  $h$ , the batch size is  $n$ , and the number of inputs is  $m$ . Thus, the input is represented as  $X_t \in R^{n \times m}$  and the hidden state at the previous moment is  $H_{t-1} \in R^{n \times h}$ . Similarly, the gates at time  $t$  have input gate  $I_t \in R^{n \times h}$ , forget gate  $F_t \in R^{n \times h}$  and output gate  $O_t \in R^{n \times h}$ . The parameter is calculated as Eq. (1).

$$\begin{cases} I_t &= \sigma(X_t W_{xi} + H_{t-1} W_{hi} + b_i) \\ F_t &= \sigma(X_t W_{xf} + H_{t-1} W_{hf} + b_f) \\ O_t &= \sigma(X_t W_{xo} + H_{t-1} W_{ho} + b_o) \end{cases} \quad (1)$$

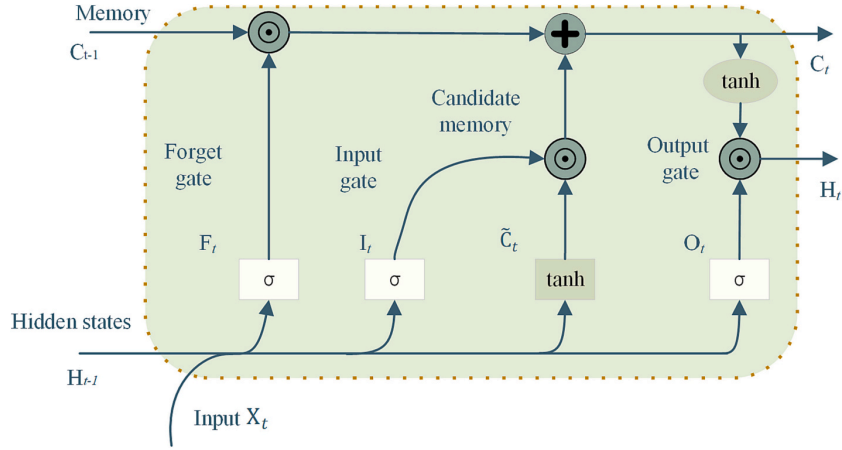


Fig. 1. The cellular structure of a single Long Short Term Memory neural network.

$W_{xi}, W_{xf}$  and  $W_{xo} \in R^{m \times h}$ , the  $W_{hi}, W_{hf}$  and  $W_{ho} \in R^{h \times h}$ , they all belong to the weight parameter.  $b_i, b_f$  and  $b_o \in R^h$ , they belong to the bias parameter.

The candidate memory element calculation is similar to the three gate calculations described above, except that the tanh function is used as the activation function and the values between  $-1$  and  $1$ . The calculation process as shown in Eq. (2). The mechanisms used to control input or forget are shown in Fig. 1. The input gate  $I_t$  controls how much new data is adopted and the forget gate  $F_t$  controls how much past data is adopted  $C_{t-1}$ .

$$\begin{cases} \tilde{C}_t = \tanh(X_t W_{xc} + H_{t-1} W_{hc} + b_c) \\ C_t = F_t \odot C_{t-1} + I_t \odot \tilde{C}_t \end{cases} \quad (2)$$

$\odot$  indicates multiplication per element,  $W_{xc} \in R^{m \times h}$  and  $W_{hc} \in R^{h \times h}$  are weight parameter,  $b_c \in R^h$  is bias parameter. In Eq. (2), if the forget gate is 1 and input gate is 0,  $C_{t-1}$  will be saved to the current moment, and the gradient disappearance problem can be effectively mitigated. Finally, the output gate in the hidden state is the gated version of tanh, which also ensures  $H_t$  is  $(-1, 1)$ , the calculation as shown in Eq. (3).

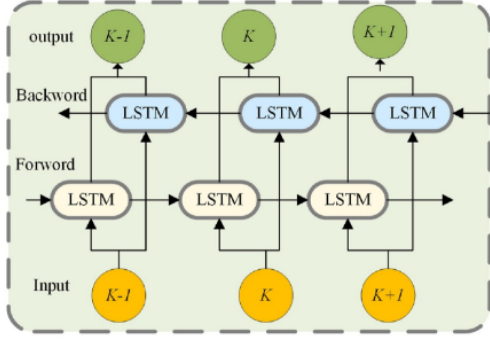
$$H_t = O_t \odot \tanh(C_t) \quad (3)$$

Interestingly, when the output gate is nearly 1, the retained memory information can be passed to the prediction section. When the output gate approaches 0, only information is retained in the memory element and the hidden state is not updated.

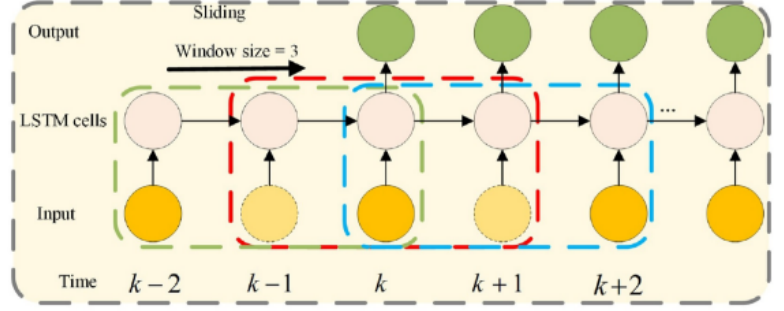
In order to make better use of LSTM, this article designs an improved Bidirectional Long Short Term Memory (BiLSTM), the algorithm has two parts forward and backward, through the forward LSTM and backward LSTM to obtain two opposite time series of hidden layer states. It can effectively enhance connection of adjacent moments. So the state of the hidden layer at moment  $t$  as Eq. (4). The BiLSTM algorithm structure as shown in Fig. 2.

$$\begin{cases} \overrightarrow{H}_t = \overrightarrow{LSTM}(H_{t-1}, X_t, C_{t-1}) \\ \overleftarrow{H}_t = \overleftarrow{LSTM}(H_{t+1}, X_t, C_{t+1}) \\ H_t = [\overrightarrow{H}_t, \overleftarrow{H}_t] \end{cases} \quad (4)$$

In BiLSTM, a single LSTM cell structure as shown in Fig. 2 (b). In most researchers' articles, the application of LSTM can be divided into single-dimensional input with single-dimensional output and multi-dimensional input with multi-dimensional output [42,43]. This article uses the underlying architecture of LSTM to design a BiLSTM network with multi-dimensional inputs to strengthen the association between current time data and past time data. To prevent the gradient explosion problem. As shown in Fig. 2 (b), the sliding window of three is designed to correlate the data well. Besides this, to better obtain a non-linear relationship between SoC and battery parameters, this paper sets the input of  $X_t = [I_t, V_t, T_t]$ ,  $I_t, V_t, T_t$  indicates Current, voltage, and temperature. Output set to real SoC.



(a) Bidirectional Long Short Term Memory structure



(b) The many-to-one structured Long Short Term Memory

Fig. 2. The many-to-one structured Bidirectional Long Short Term Memory network.

## 2.2. Rauch-Tung-Striebel-smoothing

In modern industry, Kalman Filter (KF) is often found in a variety of scenarios and used to predict the current state of system. However, in this paper, to improve the accuracy of BiLSTM estimation results, the prediction SoC results improved with the Rauch-Tung-Striebel-Smoother algorithm. The Rauch-Tung-Striebel-Smoother (RTSS) is also known as Kalman smoother. The main calculation process, as shown in Eq. (5).

$$p(x_k|y_{1:T}) = N(x_k|m_k^s, P_k^s) \quad (5)$$

In Eq. (5), usually  $T > k$ ,  $x_k$  indicates the system state at time  $k$ ,  $m_k^s$  and  $P_k^s$  indicate that the variable follows a Gaussian distribution, with a mean of  $m_k^s \in R^n$  and covariance of  $P_k^s \in R^{n \times n}$ ,  $y_{1:T}$  indicates all results observed throughout the period  $T$ . The difference between smoother and filter is also revealed, and the following will describe the backward-and- forward recurrence of smoother.

1) Forward Recursion:

$$\left\{ \begin{array}{l} x'_k = f(x_{k-1}) \\ P'_k = A_k P_{k-1} A_k^T + Q_k \\ k_k = P'_k H_k^T (H_k P'_k H_k^T + R_k)^{-1} \\ x_k = x'_k + K_k (z_k - H_k x'_k) \\ P_k = (I - K_k H_k) P'_k \end{array} \right. \quad (6)$$

In Eq. (6),  $A_k$  indicates the state transfer matrix at moment  $k$ ,  $x'_k$  indicates status estimation at moment  $k$ ,  $P'_k$  indicates the covariance matrix,  $Q$  and  $R$  are the variances of  $w$  and  $v$  respectively.  $K$  is the Kalman gain.  $I$  is the unit matrix.

2) backward Recursion:

$$\left\{ \begin{array}{l} x_{k+1}^- = A_k x_k \\ P_{k+1}^- = A_k P_k A_k^T + Q_k \\ G_k = P_k A_k^T (P_{k+1}^-)^{-1} \\ x_k^s = x_k + G_k (x_{k+1}^s - x_{k+1}^-) \\ P_k^s = P_k + G_k (P_{k+1}^s - P_{k+1}^-) G_k^T \end{array} \right. \quad (7)$$

From the initial moment to the cut-off time  $T$ , a forward recursion is completed  $T$  times, then from the moment  $T$ , a backward recursion is completed  $T$  times, then the RTSS algorithm is completed. The forward recursion process is Kalman filter and the  $x_T$  and  $P_T$  in the forward recursion result is the initial value of the backward recursion  $x_T^s$  and  $P_T^s$ .

In forward recursion of the RTSS algorithm, the input is Bidirectional LSTM estimation results, and the RTSS algorithm will reduce the error on the results. When the RTSS algorithm is finished, the SoC estimation results are again fitted as BiLSTM input. In this case, it is one-dimensional input and one-dimensional output. The input is the RTSS estimated SoC and the output is the LSTM estimated SoC. In backward recursion of RTSS algorithm, when BiLSTM is finished, the SoC estimation results as back-ward recursion of RTSS algorithm to get final SoC values.

### 2.3. Multi-constrained continuous dynamic peak power estimation

The SoP of Lithium-ion batteries describes the peak charge and discharge power that the battery can withstand at the current moment. Considering sustained peak current to be more important, this paper proposes a joint estimation method for calculating sustained peak current and peak power. By considering the results of SoC estimation, the limits of the lithium-ion battery's current limit and the limits of the terminal voltage, a multi-constrained sustained peak current and peak power estimation method is constructed. Firstly, the model-based peak current process, as shown in Eq. (8).

$$\left\{ \begin{array}{l} \hat{i}_{max,k}^{dis,L} = \frac{g(z_k, C_a) - U_{1,k} \left( \exp\left(\frac{-\Delta t}{\tau}\right) \right)^L - U_{2,k} \left( \exp\left(\frac{-\Delta t}{\tau}\right) \right)^L}{L \times \frac{\eta_i \Delta t}{C_a} \left. \frac{\partial g}{\partial z} \right|_{z=z_k} + U_{R12} + R_i} U_{t,min} \\ U_{R12} = R_1 \left( 1 - \exp\left(\frac{-\Delta t}{\tau}\right) \sum_{j=0}^{L-1} \left( \exp\left(\frac{-\Delta t}{\tau}\right) \right)^{L-1-j} \right) + R_2 \left( 1 - \exp\left(\frac{-\Delta t}{\tau}\right) \sum_{j=0}^{L-1} \left( \exp\left(\frac{-\Delta t}{\tau}\right) \right)^{L-1-j} \right) \\ \hat{i}_{min,k}^{chg,L} = \frac{g(z_k, C_a) - U_{1,k} \left( \exp\left(\frac{-\Delta t}{\tau}\right) \right)^L - U_{2,k} \left( \exp\left(\frac{-\Delta t}{\tau}\right) \right)^L - U_{t,max}}{L \times \frac{\eta_i \Delta t}{C_a} \left. \frac{\partial g}{\partial z} \right|_{z=z_k} + R_i + U_{R12}} \end{array} \right. \quad (8)$$

In Eq. (8),  $\hat{i}_{max,k}^{dis,L}$  and  $\hat{i}_{min,k}^{chg,L}$  indicates the estimation process of the sustained peak charge or discharge current based on the second order Thevenin model respectively. Second order Thevenin model as shown in Fig. 3.  $U_t$  indicates the terminal voltage of the lithium-ion batteries, where subscript min and max indicate discharge cut-off voltage and charge cut off voltage, respectively.  $\Delta t$  indicates Sample time,  $L$  indicates peak current duration.  $\tau = R_1 C_1$ ,  $g(z_k, C_a)$  indicates the non-linear relationship between open circuit voltage and SoC.

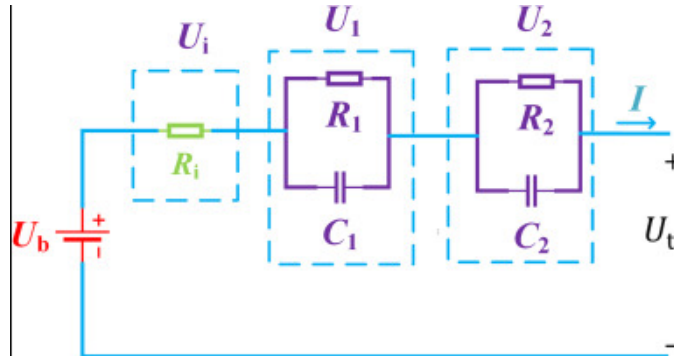


Fig. 3. Second order Thevenin model.

In Fig. 3,  $U_b$  indicates open circuit voltage.  $R_i$  indicates ohm internal resistance.  $R_1$  and  $R_2$  indicates the polarized internal resistance of the battery.  $C_1$  and  $C_2$  indicates the polarization capacitance of the battery.  $U_t$  indicates the terminal voltage of the lithium-ion batteries. The RC circuit consisting of  $R_1$  and  $C_1$  indicate the phase with fast voltage change inside the lithium-ion battery, and the RC circuit consisting of  $R_2$  and  $C_2$  indicate the phase with slow voltage change inside the lithium-ion battery. Besides this,  $R_i$  can reflect the instantaneous voltage drop caused by the sudden change of current. According to Kirchoff circuit law the circuit equation can be formulated as shown in Eq. (9).

$$\begin{cases} U_t = U_b - I(t)R_i - U_1 - U_2 \\ \frac{dU_1}{dt} = -\frac{U_1}{R_1 C_1} + \frac{I}{C_1} \\ \frac{dU_2}{dt} = -\frac{U_2}{R_2 C_2} + \frac{I}{C_2} \end{cases} \quad (9)$$

Second. Given the maximum and minimum limits of SoC, the SoC peak current calculation process for lithium-ion battery, as shown in Eq. (10).

$$\begin{cases} \hat{i}_{min,k}^{chg,zL} = \frac{z_k - z_{max}}{L \times \eta_i \Delta t / C_a} \\ \hat{i}_{max,k}^{dis,zL} = \frac{z_k - z_{min}}{L \times \eta_i \Delta t / C_a} \end{cases} \quad (10)$$

$\hat{i}_{min,k}^{chg,zL}$  and  $\hat{i}_{max,k}^{dis,zL}$  are the estimated sustained peak charge/discharge current based on the SoC at time  $k$ , respectively.  $L$  indicates the duration of the peak current, and when  $L = 1$  indicates the instantaneous peak power.  $z_k$  indicates SoC estimated result at  $k$ .  $z_{max}$  and  $z_{min}$  indicate the limit value of SoC. The calculation of the multi-constrained sustained peak current is obtained by combining Eqs. (8) and (10), as shown in Eq. (11).

$$\begin{cases} \hat{I}_{min,k}^{chg,L} = \min\{I_{min}, \hat{i}_{min,k}^{chg,zL}, \hat{i}_{min,k}^{chg,L}\} \\ \hat{I}_{max,k}^{dis,L} = \max\{I_{max}, \hat{i}_{max,k}^{dis,zL}, \hat{i}_{max,k}^{dis,L}\} \end{cases} \quad (11)$$

$\hat{I}_{min,k}^{chg,L}$  and  $\hat{I}_{max,k}^{dis,L}$  are the peak charge and discharge currents under multiple constraints, respectively. According to Eq. (11), it is possible to obtain an estimate of the continuous charge and discharge power, as shown Eq. (12).

$$\begin{cases} \hat{P}_{max,k}^{chg,L} = \max\{P_{min}, U_{t,k+L}(\hat{I}_{min,k}^{chg,L}) \times \hat{I}_{min,k}^{chg,L}\} \\ \hat{P}_{max,k}^{dis,L} = \min\{P_{max}, U_{t,k+L}(\hat{I}_{max,k}^{dis,L}) \times \hat{I}_{max,k}^{dis,L}\} \\ U_{t,k+L} = g(z_k, C_a) - \left[ \left( \exp\left(\frac{-\Delta t}{\tau}\right) \right)^L U_{1,k} + \right. \\ \left. i_{L,k} R_1 \left( 1 - \exp\left(\frac{-\Delta t}{\tau}\right) \right) \sum_{j=0}^{L-1} \left( \exp\left(\frac{-\Delta t}{\tau}\right) \right)^{L-1-j} \right] + \\ \left[ \left( \exp\left(\frac{-\Delta t}{\tau}\right) \right)^L U_{2,k} + i_{L,k} R_2 \left( 1 - \exp\left(\frac{-\Delta t}{\tau}\right) \right) \sum_{j=0}^{L-1} \left( \exp\left(\frac{-\Delta t}{\tau}\right) \right)^{L-1-j} \right] - i_{L,k} R_i \end{cases} \quad (12)$$

In Eq. (12),  $\hat{P}_{max,k}^{chg,L}$  and  $\hat{P}_{max,k}^{dis,L}$  are the peak discharge power and peak charge power estimated by the multi-constrained sustained peak power estimation method at time  $k$ , respectively. The entire flow chart of the algorithm as shown in Fig. 4.

In Fig. 4, K and T indicate the current moment. K-1 and T-1 indicate the previous moment. The entire algorithm operates in the following steps. Firstly, the BMS collects the current, voltage and temperature of the lithium-ion battery. Secondly, the three parameters are fitted to the true SoC by the proposed BiLSTM-RTSS algorithm to obtain the estimated SoC. In this process, the state variable SoC in  $x_k$  will sent to the lstm cell for the next fit. Thirdly, the SoC, the battery current limit, and the second order RC model current limit are used as constraints to estimate the sustained peak current and peak power. The joint estimation of SoC and SoP is finally obtained.

### 3. Experimental analysis

#### 3.1. Lithium-ion battery test platform design

In this paper, the experiment is conducted using a 70 Ah ternary lithium-ion battery. The experimental configuration is divided into six parts: Temperature test chamber, charge and discharge test, lithium-ion battery, PC, CAN and BMS, as shown in Fig. 5.

This article utilizes the system configuration to perform Hybrid Pulse Power Characterization (HPPC) test and Beijing Bus Dynamic Stress Test (BBDST) test of lithium-ion batteries in a multi-temperature environment. To subvalidate the proposed algorithms, the test environments are divided into 15, 25, and 35 degrees. The test results as shown in Fig. 6.

In Fig. 6, the first groups are BBDST tests, recording voltage and current at 15, 25, and 35 degrees, respectively. The last groups are HPPC tests at 25 and 35 degrees. This paper uses the BBDST data at 25 degrees to verify the BiLSTM-RTSS algorithm and calculate the maximum sustained peak power and current.

### 3.2. Improved M-1 BiLSTM-RTSS algorithm verification under BBDST and HPPC

The training dataset of BiLSTM algorithm is BBDST data at an ambient temperature of 25 degrees, and the BBDST data at 15 and 35 degrees and HPPC data under 25 and 35 degrees are used as the test dataset, respectively. The algorithm consisted of three layers, the BiLSTM layer, the dropout layer, and the dense layer. The Mean Squared Error (MSE) is used as the loss function and Adam is used as the optimiser. In terms of parameter settings, more layers of BiLSTM are not better, only one layer of BiLSTM effect is already very well because Bidirectional LSTM includes two LSTM that is forward and backward. When BiLSTM has overfitting, the Dropout layer is used to randomly remove neural units to suppress overfitting, and a ratio of 0.2 is chosen in this paper.

The LSTM configuration is approximately the same as the BiLSTM parameters in this paper, the difference is that the LSTM has 100 learning cycles and the BiLSTM has 40 learning cycles for the first and 20 for the second. It can be quickly combined with the RTSS algorithm to reduce the training time and improve the training accuracy.

In the paper, to verify the accuracy of the improved M-1 structured BiLSTM-RTSS algorithm, the traditional algorithms are also introduced

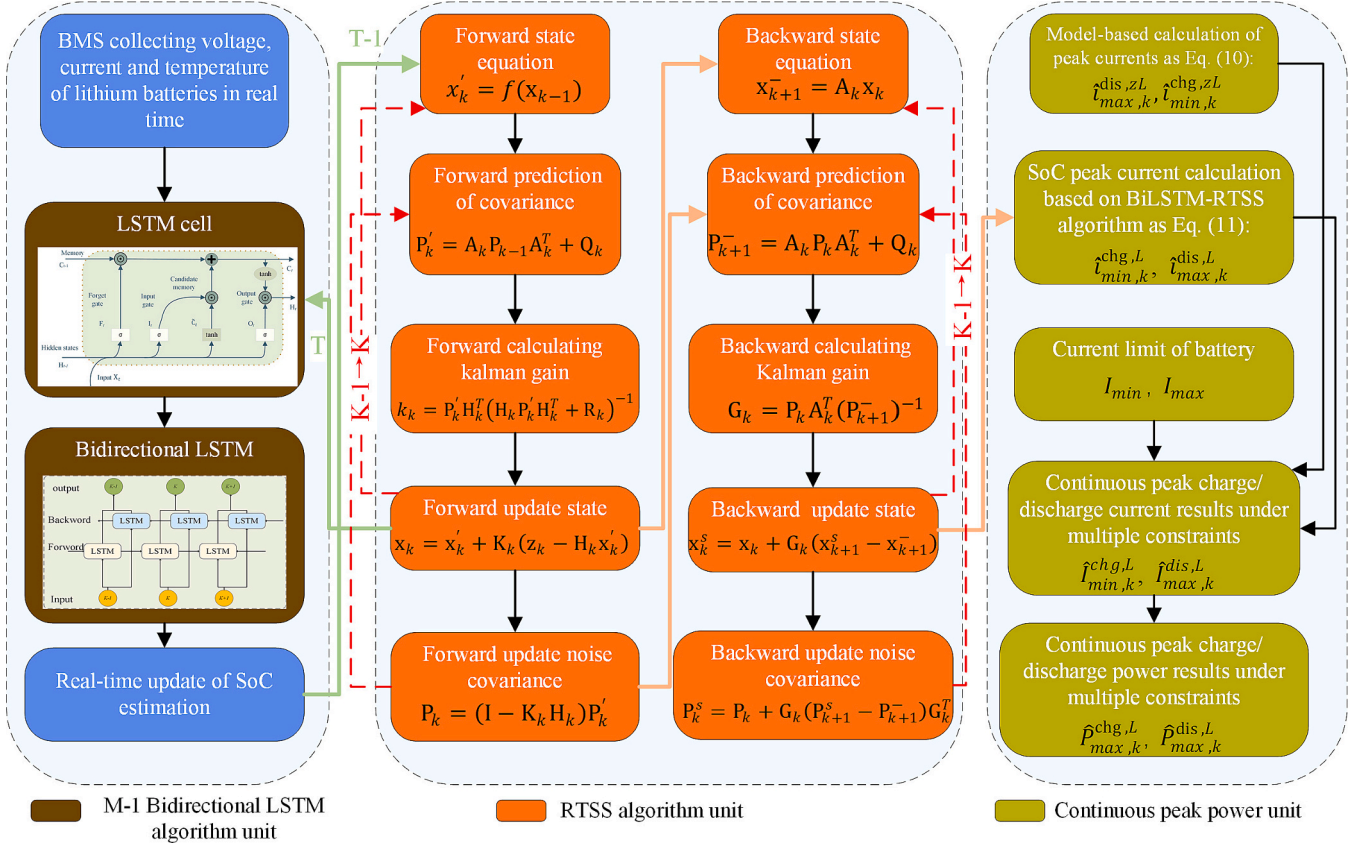


Fig. 4. Algorithm framework for M-1 structured Bidirectional Long Short Term Memory based on Rauch Tung Striebel Smoothing.

for comparison, including Long Short Term Memory, Support Vector Machine (SVM), and the Extend Kalman Filter (EKF) algorithm, the results as shown in Fig. 7. The algorithms running time, as shown in Table 1.

In Table 1, BiLSTM-RTSS and EKF spend similar running time, which is due to the EKF not requiring training time. So BiLSTM-RTSS algorithm has a "quickly" character.

From Table 1, the BiLSTM-RTSS algorithm takes a maximum time of 10 min and the LSTM takes the minimum time of 24 min. The running

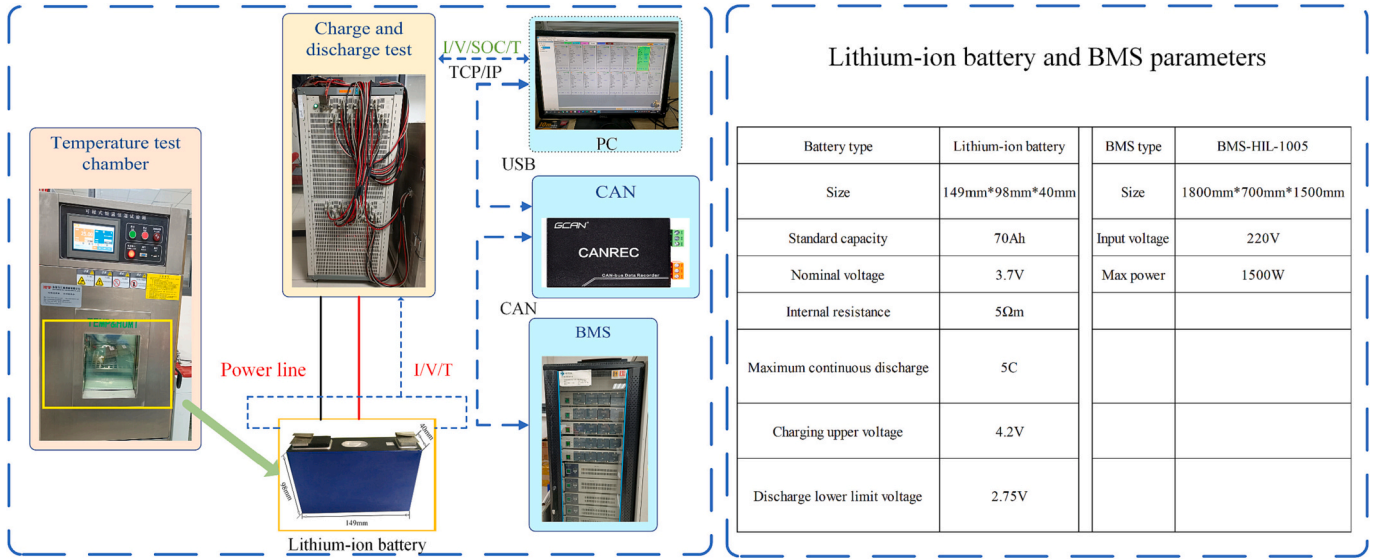


Fig. 5. Lithium-ion battery test platform and parameters.

time of the BiLSTM-RTSS algorithm is half of the LSTM algorithm, reflecting the quickly of the BiLSTM-RTSS algorithm.

To reflect the accuracy of the BiLSTM-RTSS algorithm, the initial value of all SoC of the algorithm is set to 1. In Fig. 7 (a) and (c), it can be seen that the convergence and stability of the BiLSTM-RTSS algorithm is better than the other algorithm. In Fig. 7 (b) and (d), (f) and (h), BBDST conditions under 15 and 35 degrees the maximum error of the BiLSTM-RTSS algorithm is 0.0184 and 0.0150, which keep approaching the true value during the iterations. The maximum error of the LSTM algorithm is 0.0307 and 0.0277, with fluctuations getting larger. The maximum error of SVM algorithm is 0.0409 and 0.0400. The maximum error of the EKF algorithm is 0.0597 and 0.0927. From Fig. 7 (f) and (h), HPPC conditions under 25 and 35 degrees the maximum error of the BiLSTM-RTSS algorithm is 0.0229 and 0.0165. The maximum error of the LSTM algorithm is 0.0233 and 0.0223. The maximum error of SVM algorithm is 0.0429 and 0.0504. The maximum error of the EKF algorithm is 0.0799 and 0.1116. Besides this, this paper uses Mean Absolute Error (MAE) to evaluate the effectiveness of algorithms, as shown in Table 2.

Table 1  
Running time of the algorithm.

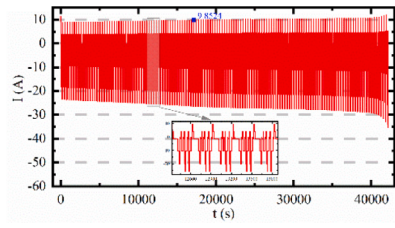
	BBDST (15 °C)	BBDST (35 °C)	HPPC (25 °C)	HPPC (35 °C)
BiLSTM-RTSS (min)	8	10	9	8
LSTM (min)	25	26	24	25
SVM (min)	20	21	19	20
EKF (min)	7	9	9	10

Table 2  
MAE results of the algorithm.

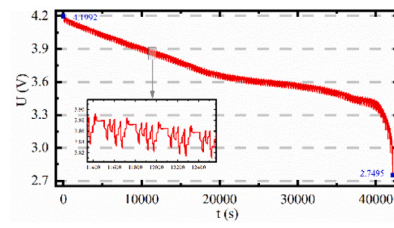
Work condition	BiLSTM-RTSS (%)	LSTM (%)	SVM (%)	EKF (%)
BBDST under 15 degrees	0.548	0.851	1.19	2.928
BBDST under 35 degrees	0.469	0.790	0.881	4.107
HPPC under 25 degrees	0.619	0.929	1.249	1.369
HPPC under 35 degrees	0.602	0.861	1.235	2.738

Table 3  
Constraint values for lithium-ion battery.

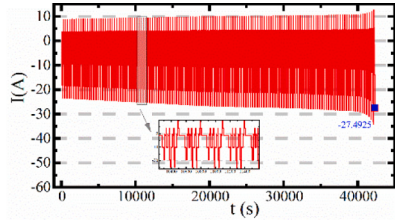
Parameter	Max	Min
SoC	1	0.2
U (V)	4.2	2.75
I (A)	450	-170
P (W)	1200	-460



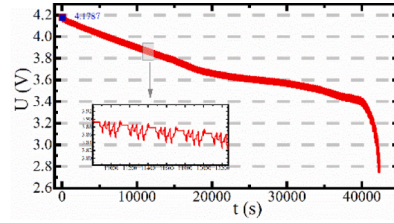
(a) BBDST current test under 15 degree



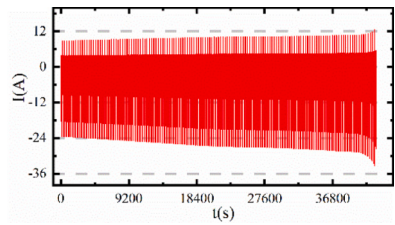
(b) BBDST voltage test under 15 degree



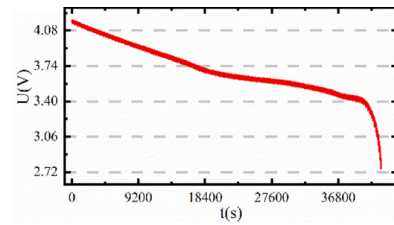
(c) BBDST current test under 25 degree



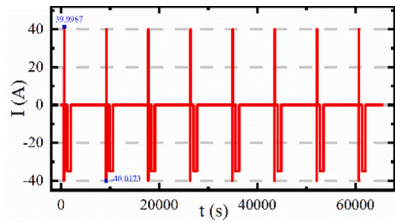
(d) BBDST voltage test under 25 degree



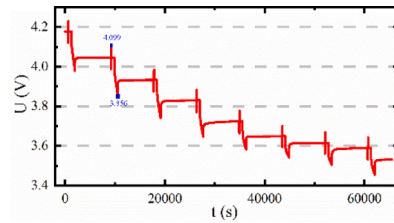
(e) BBDST current test under 35 degree



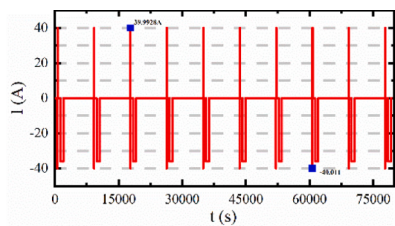
(f) BBDST voltage test under 35 degree



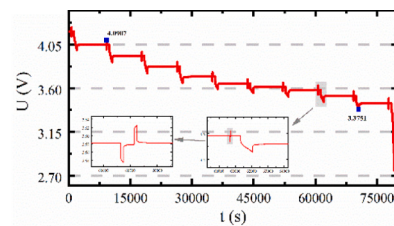
(g) HPPC current test under 25 degree



(h) HPPC voltage test under 25 degree

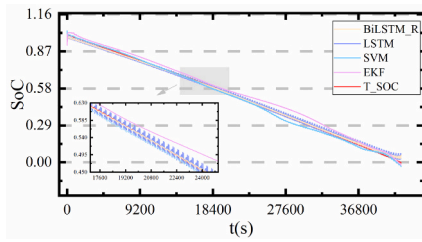


(i) HPPC current test under 35 degree

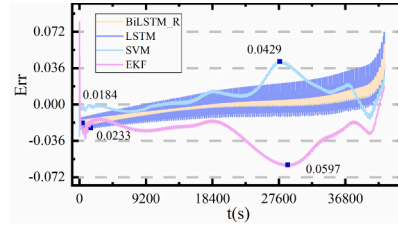


(j) HPPC voltage test under 35 degree

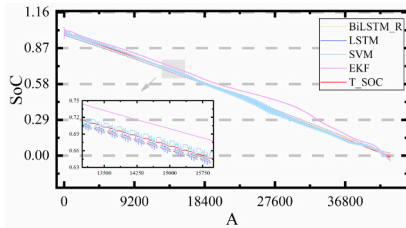
Fig. 6. HPPC and BBDST current and voltage tests at ambient temperatures of 15, 25 and 35 degrees.



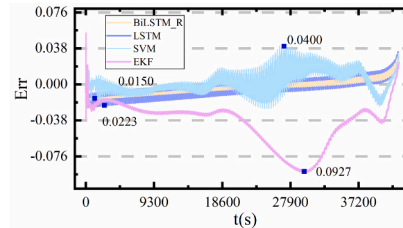
(a) Comparison BBDST condition algorithms at 15 degree



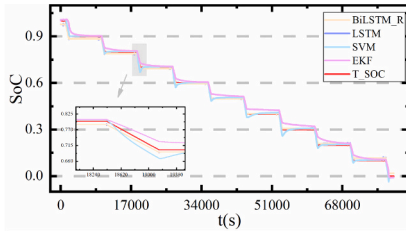
(b) Algorithm comparison error



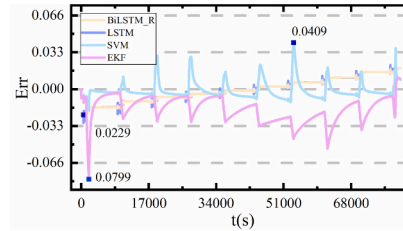
(c) Comparison BBDST condition algorithms at 35 degree



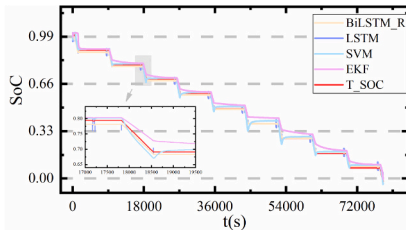
(d) Algorithm comparison error



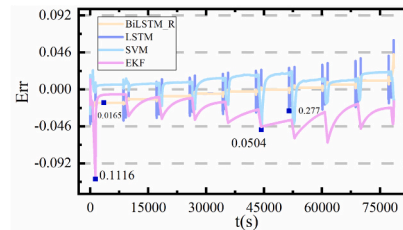
(e) Comparison HPPC condition algorithms at 25 degree



(f) Algorithm comparison error



(g) Comparison HPPC condition algorithms at 35 degree



(h) Algorithm comparison error

Fig. 7. Results of the M-1structured BiLSTM-RTSS, LSTM, SVM and EKF algorithms in a multi-temperature environment.

### 3.3. Continuous peak charge/discharge power with multiple constraints

The HPPC test results under 25 degrees are selected as the model constraint. The SoC estimated by the M-1 structured BiLSTM-RTSS algorithm is used as the second constraint. The limit value of the battery is used as the third constraint. The constraint values of lithium-ion battery, as shown in Table 3. In this paper, SoC values below 0.2 are unrealistic in real life, so SoC data for the 0.2–1 interval is used only. Besides this, real SoC is used as one of the constraints, and estimated peak current and power are used as reference values. The sustained peak power and charge/discharge currents are described for the 30 s, 2 min, and 4 min, respectively. The results as shown in Fig. 8 and Fig. 9. The Mean Absolute Error (MAE) and Root Mean Square Error (RMSE) were chosen as error evaluation indicators to evaluate the peak current and peak power, respectively, as shown in Fig. 10.

Fig. 8 (a) shows the constraint process for the current based on the three constraints. It shows that when SoC approaches the maximum limit, the peak current based on the SoC value will reduce or turn off the charge current to prevent the battery from being overcharged. This process is mainly determined based on the SoC constraint. In the other processes, the current values are consistent with the OCV-based constraint current values. In Fig. 8 (b), the peak current based on OCV maximum estimation error is 1.7 A, the based on SoC maximum estimation error is 60 A, and the maximum current estimation error based on three constraints is 7.952 A.

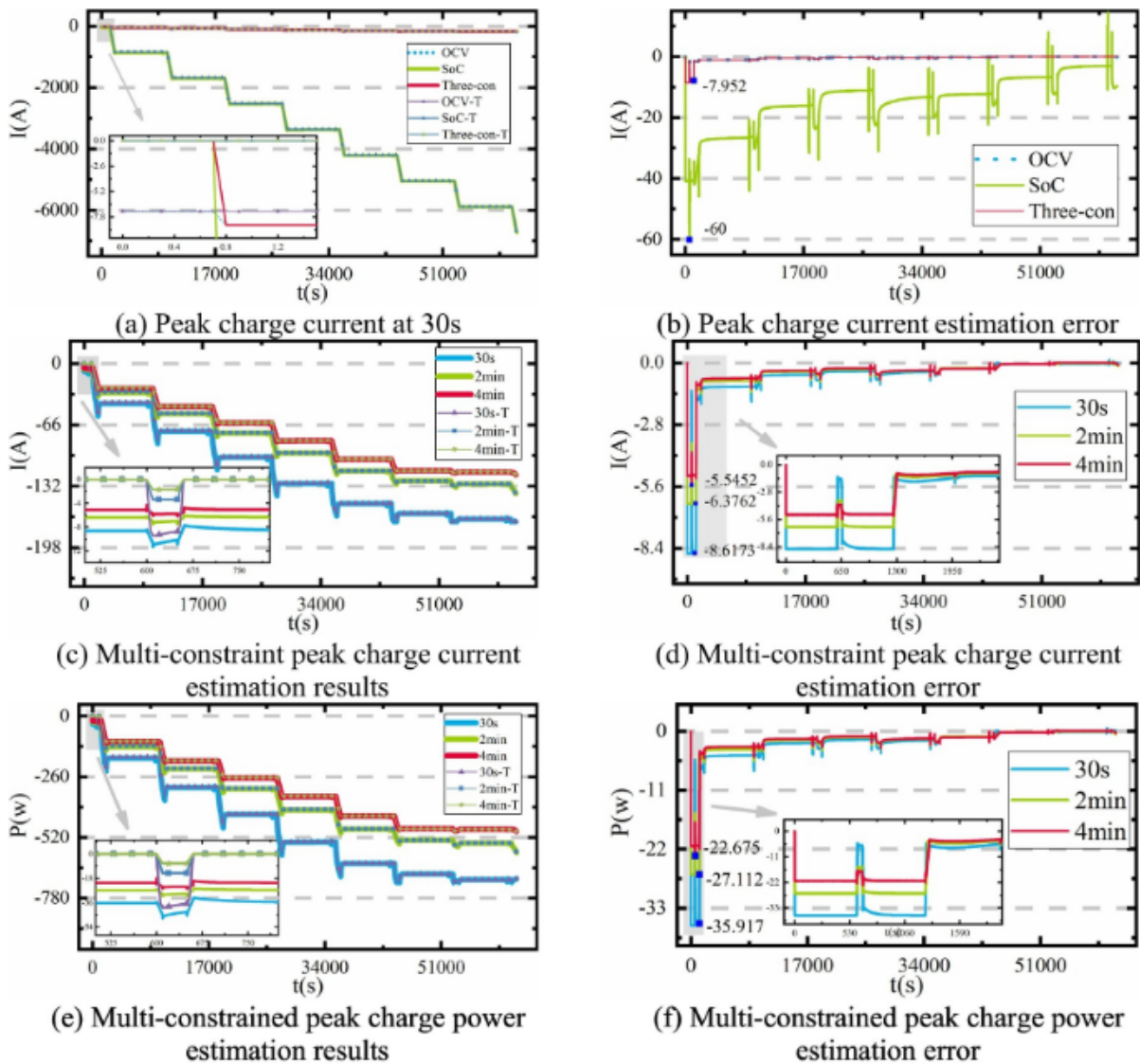


Fig. 8. Continuous peak charge current and power under three constraints.

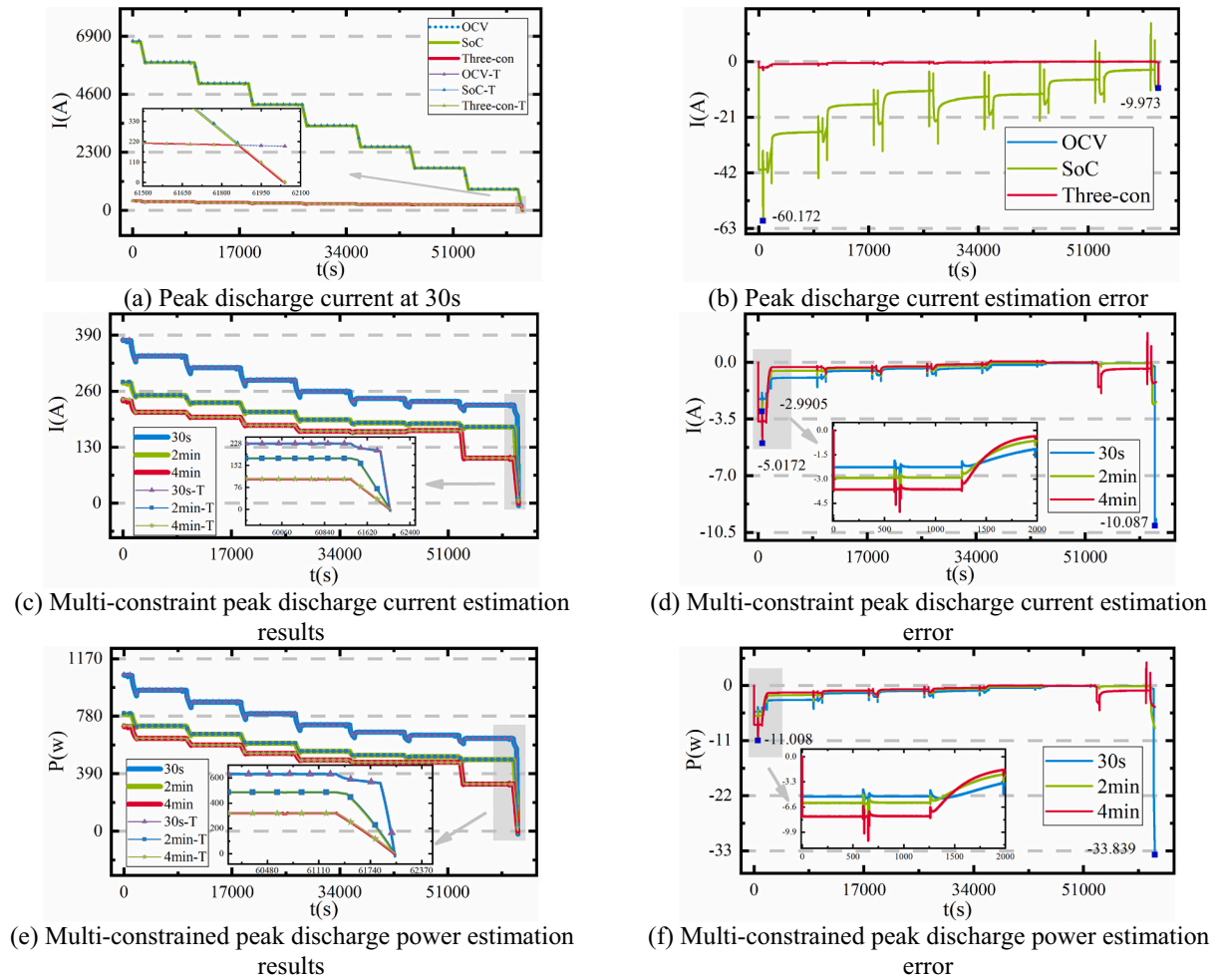


Fig. 9. Continuous peak discharge current and power under three constraints.

Fig. 8 (c) shows that peak charge current highly depends on the sustained output time. When the sustained output time is 30 s, 2 min and 4 min, the peak charge current reaches 165 A, 139 A and 119 A, respectively. As can be seen, the current does not exceed the limit value, and the maximum peak charge current decreases with increased continuous output time. Besides this, the estimated peak current maximum errors at the 30 s, 2 min and 4 min sustained durations are 8.6173 A, 6.3762 A and 5.5452 A.

Fig. 8 (e) shows a consistent trend in sustained peak power and current. The maximum peak power is 697 W, 583 W and 491 W at a sustained duration of the 30 s, 2 min and 4 min. Similarly, the maximum peak charging power decreases with increasing time. Besides this, the estimated peak power maximum errors at the 30 s, 2 min and 4 min sustained durations are 35.917 W, 27.112 W and 22.675 W. The results are highly accurate for peak current and power estimation.

Through the above analysis, the algorithm has high accuracy and reliability in the peak charge calculations. No specified limit is exceeded, and the peak charge ability decreases with increasing sustained duration. The algorithm can effectively protect the battery during the charging process.

Similar to charge, when SoC approaches the minimum limit, the peak current based on the SoC value will reduce or turn off the discharge current to prevent the battery from overdischarged. This process is also mainly determined based on the SoC constraint. Besides this, when the sustained duration is 30 s, 2 min and 4 min, the maximum peak discharge current reaches 380 A, 281 A and 241 A, and the error is 10.087 A, 5.0172 A and 2.9905 A, respectively. And the maximum peak discharge power reaches 1062 W, 800 W and 715 W, and the error is 33.839 W, 11.008 W and 8.7036 W, respectively. According to the data, the ability of the peak discharge current and peak discharge power also decreases with increasing duration.

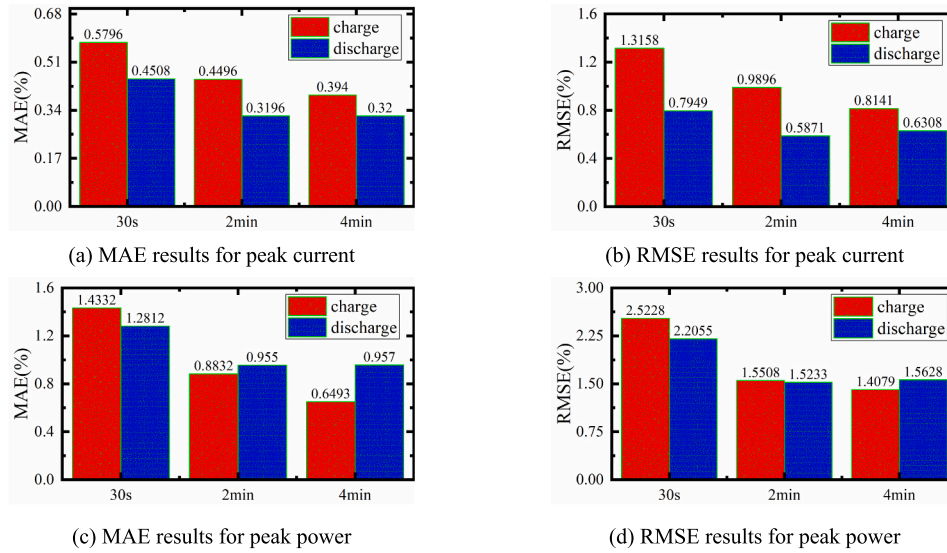


Fig. 10. Peak charge/discharge power and current MAE and RMSE calculation results.

Obviously, with the SoC value decreasing, the peak charge current becomes larger and the peak discharge current becomes smaller. Still, neither exceeds the limiting current, including a maximum peak current of 450 A and a minimum peak current of 170 A. So the SoC-based constraints can effectively avoid the danger of overcharging and over-discharging and improve the safety of lithium-ion batteries. Of course, this result requires an accurate SoC estimation, so a BiLSTM-RTSS algorithm is essential.

Fig. 10 shows that the maximum MAE of peak charge current and power are 0.5796 % and 1.4332 %, respectively. The maximum peak charge current and power RMSE are 1.3158 % and 2.5055 %, respectively. The analysis shows that the MAE and RMSE remain at a small value and the algorithm is reliable. The estimation results do not depend on only one constraint and the peak charge or discharge power is not affected when there is a significant error in one constraint.

#### 4. Conclusions

This paper focuses on the reliable, stable and efficient estimation of the SoC and SoP of the lithium-ion battery. A novel M-1 structured Bidirectional Long Short Term Memory neural network combined with Rauch Tung Striebel Smoothing algorithm is proposed to estimate SoC, which can effectively fit current, voltage, temperature and SoC by using the improved sliding window M-1 technique. The RTSS algorithm is applied to update the SoC estimation of the BiLSTM to facilitate the accuracy and speed of SoC estimation. The maximum estimation error of SoC is 0.0184 and 0.0229 respectively under BBDST and HPPC conditions. In the SoP estimation, three key constraints including SoC, second-order RC model and battery limits are established. When the duration is 30s, the peak charging and discharging currents are up to 170A and 380A. The results can directly reflect the sustained peak charge/ discharge current characteristics under the multi-constrained conditions and obtain the sustained peak power in the same trend as the sustained peak current. The estimation results show that the algorithm has high accuracy and robustness.

#### CRedit authorship contribution statement

**Tao Long:** Writing, Original draft preparation, Software  
**Shunli Wang:** Data curation, Conceptualization, Methodology  
**Wen Cao:** Visualization, Investigation  
**Heng Zhou:** Software, Validation  
**Carlos Fernandez:** Supervision  
**Yangtao Wang:** Drawing, proofreading

#### Declaration of competing interest

The authors declare that they have no known competing financial interests or personal relationships that could have appeared to influence the work reported in this paper.

#### Data availability

Data will be made available on request.

#### Acknowledgments

The work was supported by National Natural Science Foundation of China (No. 62173281, 61801407).

## References

- [1] A. Kalair, et al., Role of energy storage systems in energy transition from fossil fuels to renewables, *Energy Storage* 3 (1) (2021) 20–35.
- [2] S. Kirsch, Running out? Rethinking resource depletion, *Extr. Ind. Soc. Int. J.* 7 (3) (2020) 838–840.
- [3] P. Reimers, The subsidized green revolution: the impact of public incentives on the automotive industry to promote alternative fuel vehicles (AFVs) in the period from 2010 to 2018, *Energies* 14 (18) (2021) 545–592.
- [4] A. Biernat-Jarka, P. Trebska, S. Jarka, The role of renewable energy sources in alleviating energy poverty in households in Poland, *Energies* 14 (10) (2021) 1066–1082.
- [5] M.M. Nezhad, et al., Green energy sources assessment using Sentinel-1 satellite remote sensing, *Front. Energy Res.* 9 (2021) 800–822.
- [6] T. Zhang, et al., Increasing urban tram system efficiency, with battery storage and electric vehicle charging, *Transp. Res. Part D: Transp. Environ.* 80 (2020) 458–502.
- [7] D. Li, et al., Temperature prediction of lithium-ion batteries based on electrochemical impedance spectrum: a review, *Int. J. Energy Res.* 15 (18) (2022) 854–870.
- [8] T.L. Kulova, et al., A brief review of post-lithium-ion batteries, *Int. J. Electrochem. Sci.* 15 (8) (2020) 7242–7259.
- [9] M. Armand, et al., Lithium-ion batteries - current state of the art and anticipated developments, *J. Power Sources* 479 (2020) 1527–1559.
- [10] M. Naguib, P. Kollmeyer, A. Emadi, Lithium-ion battery pack robust state of charge estimation, cell inconsistency, and balancing: review, *IEEE Access* 9 (2021) 50570–50582.
- [11] I.B. Espedal, et al., Current trends for state-of-charge (SoC) estimation in lithium-ion battery electric vehicles, *Energies* 14 (11) (2021) 668–710.
- [12] X. Xiong, et al., A novel practical state of charge estimation method: an adaptive improved ampere-hour method based on composite correction factor, *Int. J. Energy Res.* 44 (14) (2020) 11385–11404.
- [13] Z. Zhou, et al., A fast capacity estimation method based on open circuit voltage estimation for LiNiCoMn1-x-y battery assessing in electric vehicles, *J. Energy Storage* 32 (2020) 1204–1224.
- [14] R.X. Liu, C.L. Zhang, An active balancing method based on SOC and capacitance for lithium-ion batteries in electric vehicles, *Front. Energy Res.* 9 (2021) 774–795.
- [15] M. Gholizadeh, A. Yazdizadeh, Systematic mixed adaptive observer and EKF approach to estimate SOC and SOH of lithium-ion battery, *IET Electr. Syst. Transp.* 10 (2) (2020) 135–143.
- [16] M.T. Huang, Q.B. Zhang, IEEE, Prediction of Remaining Useful Life of Lithium-ion Battery Based on UKF, Chinese Automation Congress (CAC), Shanghai, PEOPLES R CHINA, 2020.
- [17] X. Shu, et al., State of health prediction of lithium-ion batteries based on machine learning: advances and perspectives, *Iscience* 24 (11) (2021).
- [18] C. Janiesch, P. Zschech, K. Heinrich, Machine learning and deep learning, *Electron. Mark.* 31 (3) (2021) 685–695.
- [19] R. Roscher, et al., Explainable machine learning for scientific insights and discoveries, *IEEE Access* 8 (2020) 42200–42216.
- [20] S. Jafari, et al., Lithium-ion battery estimation in online framework using extreme gradient boosting machine learning approach, *Mathematics* 10 (6) (2022) 587–610.
- [21] S. Shen, et al., Deep convolutional neural networks with ensemble learning and transfer learning for capacity estimation of lithium-ion batteries, *Appl. Energy* 260 (2020) 1458–1482.
- [22] M.A. Hannan, et al., Toward enhanced state of charge estimation of lithium-ion batteries using optimized machine learning techniques, *Sci. Rep.* 10 (1) (2020) 875–901.
- [23] Y.F. Liu, et al., State of charge estimation of lithium-ion batteries based on temporal convolutional network and transfer learning, *IEEE Access* 9 (2021) 34177–34187.
- [24] J.L. Chen, et al., An improved gated recurrent unit neural network for state-of-charge estimation of lithium-ion battery, *Appl. Sci.-Basel* 12 (5) (2022) 784–810.
- [25] F. Zhao, et al., Lithium-ion batteries state of charge prediction of electric vehicles using RNNs-CNNs neural networks, *IEEE Access* 8 (2020) 98168–98180.
- [26] C. Bian, H.L. He, S.K. Yang, Stacked bidirectional long short-term memory networks for state-of-charge estimation of lithium-ion batteries, *Energy* 191 (2020) 1956–1981.
- [27] R.H. Guo, W.X. Shen, A review of equivalent circuit model based online state of power estimation for lithium-ion batteries in electric vehicles, *Vehicles* 4 (1) (2022) 1–29.
- [28] J. Duan, et al., Building safe lithium-ion batteries for electric vehicles: a review, *Electrochem. Energy Rev.* 3 (1) (2020) 1–42.
- [29] Y.Q. Tan, et al., Joint estimation of ternary lithium-ion battery state of charge and state of power based on dual polarization model, *Int. J. Electrochem. Sci.* 15 (2) (2020) 1128–1147.
- [30] C.H. Liu, et al., State of power estimation of lithium-ion battery based on fractional-order equivalent circuit model, *J. Energy Storage* 41 (2021) 458–472.
- [31] P.J. Qin, et al., Joint SOC-SOP estimation method for lithium-ion batteries based on
- [32] X. Shu, et al., An adaptive multi-state estimation algorithm for lithium-ion batteries incorporating temperature compensation, *Energy* 207 (2020).
- [33] T. Zhang, et al., A systematic framework for state of charge, state of health and state of power co-estimation of lithium-ion battery in electric vehicles, *Sustainability* 13 (9) (2021).
- [34] H. Sun, et al., Data-driven ICA-bi-LSTM-combined lithium battery SOH estimation, *Math. Probl. Eng.* 2022 (2022), 9645892.
- [35] T.E. Fan, et al., Simultaneously estimating two battery states by combining a long short-term memory network with an adaptive unscented Kalman filter, *J. Energy Storage* (2022) 50.
- [36] D.Z. Li, et al., Aging state prediction for supercapacitors based on heuristic kalman filter optimization extreme learning machine, *Energy* 250 (2022).  
electro-thermal model and multi-parameter constraints, *J. Power Electron.* 22 (3) (2022) 490–502.
- [37] S. Dong, P. Wang, K. Abbas, A survey on deep learning and its applications, *Comput. Sci. Rev.* 40 (2021) 740–764.
- [38] Z.H. Cui, et al., A comprehensive review on the state of charge estimation for lithium-ion battery based on neural network, *Int. J. Energy Res.* 46 (5) (2022) 5423–5440.
- [39] W. He, et al., Boosting the electrochemical performance of Li- and Mn-rich cathodes by a three-in-one strategy, *Nano-Micro Lett.* 13 (1) (2021).
- [40] X.Q. Ren, et al., A method for state-of-charge estimation of lithium-ion batteries based on PSO-LSTM, *Energy* 234 (2021).
- [41] H.X. Tian, J.H. Chen, Deep learning with spatial attention-based CONV-LSTM for SOC estimation of lithium-ion batteries, *Processes* 10 (11) (2022).
- [42] R. Yan, et al., Multi-hour and multi-site air quality index forecasting in Beijing using CNN, LSTM, CNN-LSTM, and spatiotemporal clustering, *Expert Syst. Appl.* 169 (2021) 897–921.
- [43] H.F. Zheng, et al., A hybrid deep learning model with attention-based conv-LSTM networks for short-term traffic flow prediction, *IEEE Trans. Intell. Transp. Syst.* 22 (11) (2021) 6910–6920.